Simulating phase contrast imaging for materials with variable density (PART II)

Ana C. Fabela Hinojosa

Supervisors: Assoc. Prof. Marcus Kitchen

September 21, 2021,
Due date: Friday 23$^{\text{th}}$ September, 2021

1 Current objective

In this project I study the theoretical perspective of coherent X-ray imaging by creating several simulations of cylinder shaped sample materials subject to different energy X-ray wave-fields. In some of my simulations I use a single cylinder made of a monomorphic material and in others I use two embedded concentric cylinder shaped samples of materials with either an equal chemical composition and different densities or different chemical composition and the same density. The goal of making these simulations is to verify if and how distinctly phase contrast occurs from a sample of two different brain material samples of grey and white matter under the same wave-field. and whether the observed phase contrast is density dependent. The aim is to verify if successful phase retrieval can be done of the imaged objects given variable sample material densities.

2 Theory fundamentals

For the single cylinder simulations I use the projection approximation to solve a partial differential equation known as the transport-of-intensity equation (TIE). This equation is used to quantify the contrast (i.e. refractive (phase) effects) present in propagation-based X-ray phase contrast images[1].

$$-\nabla_T[I(x,y,z)\nabla_T\phi(x,y,z)] = k\frac{\partial I(x,y,z)}{\partial z}, \tag{1}$$

here k is the wave-number, $I(x,y,z)$ is the intensity and $\phi(x,y,z)$ is the phase of the X-ray beam. The projection approximation takes into account X-ray–matter interaction therefore, the position dependent and complex form for the refractive index is introduced: $n(x,y,z) = 1 - \delta(x,y,z) + i\beta(x,y,z)$. The real part of this complex quantity corresponds to the refractive index while the imaginary part is related only to the absorptive properties of the sample[1]. Under the projection approximation, the Beer-Lambert law of attenuation is used to describe the intensity attenuation due to the sample

$$I(x,y,z_0) = \exp[-\int_t \mu(x,y,z)dz]I(x,y,0), \tag{2}$$

where $\mu = 2k\beta$ is the *linear attenuation coefficient* of the sample; μ is a function of the imaginary part of the sample's complex refractive index. The real part of the complex refractive index (δ) is known as the refractive index decrement, it physically describes phase-shifts of each wave-front coordinate which continuously accumulate in the direction of the light propagation.

$$\Delta\phi(x,y) = -k\int_t \delta(x,y,z)dz, \tag{3}$$

here t is the projected thickness of the object in the direction of the light flow. The TIE effects observable changes onto the intensity (eq.2) and phase (eq.3) after these are used as the initial conditions of the propagation problem.

To implement the spatial evolution in the direction of the light propagation, I use fourth-order Runge-Kutta with the TIE. I wrote the Runge-Kutta evolution algorithm as

$$
\begin{aligned}
k_1 &= f(z, I_n, \phi), \\
k_2 &= f(z + \frac{\Delta z}{2}, I_n + \frac{1}{2}k_1, \phi)), \\
k_3 &= f(z + \frac{\Delta z}{2}, I_n + \frac{1}{2}k_2, \phi)), \\
k_4 &= f(z + \Delta z, I_n + k_3, \phi)), \\
I_{n+1} &= I_n + \frac{1}{6}(k_1 + 2k_2 + 2k_3 + k_4) + O(\Delta z^5),
\end{aligned}
\tag{4}
$$

where I set $\Delta z = 1$mm as the spatial evolution step. The propagation via fourth order Runge-Kutta over a spatial interval is done by solving a differential equation f using four Euler-style steps, i.e. the k_i coefficients, where each Euler-style step involves one evaluation of the differential equation with slightly different input parameters. The method combines the information obtained for each solution to match a Taylor series expansion up to fourth order. the combined evaluations of the differential equation eliminate the error terms order by order, leaving the error remaining being very small[2].

For the two cylinder simulations I also use the projection approximation but this time I model the propagation of the X-ray monochromatic wave-field using a method known as the angular spectrum formulation (ASF). This method uses Fourier decomposition of wave-fields at a single plane into distinct component plane waves. Each plane wave component is propagated through the Fourier domain to a destination plane and then the propagated wave-field components are reconstructed via an inverse spatial Fourier transform[3]. To implement the ASF I use the X-ray imaging XRI library, since their algorithm has already implemented several fixes to undesirable instabilities that can appear in the simulations. This library was built by the Monash X-ray imaging group.

2.1 Imaging brain materials

Current knowledge about the properties of grey and white matter is that these are optically extremely similar. However, it is known that there is a small difference in the values of the attenuation coefficients of these materials. In previous work done by my supervisor and other members of the X-ray imaging group, CT brain imaging has been reported to yield clearly demarcated tissue borders at the grey/white matter boundaries[4]. I want to verify whether X-ray imaging grey and white matter can also yield visible phase contrast fringes. My goal is to verify if the observed boundaries in Beltran et al.(2011) (see reference [4]) are due to a density difference between grey and white matter, or whether the boundaries are solely due to the materials being chemically different.

To simulate grey and white matter I use the attenuation coefficients for both materials $\mu_{GM,WM}$ obtained by CT imaging data acquired at Japan's SPring-8 synchrotron radiation facility using an X-ray energy of $E = 24$keV and a sample-to-detector distance of 5m[5]. In my calculations I also use some experimental grey and white matter densities reported in the "IT'IS Database for thermal and electromagnetic parameters of biological tissues". To find the complex refractive index components of the whole brain (i.e. δ_B and μ_B) under certain energy X-rays, I use the X-ray imaging group "X-ray attenuation calculator" which employs the values recorded in NIST in database 66[6] making these easily accessible via GUI program, (note: I use this specific tool in all my simulations, not only the ones pertaining the brain materials). Using all these tools I calculated an approximate estimate for the grey and white matter corresponding refractive index decrements (δ_{GM} and δ_{WM}) The calculations were simple, in one I modelled the refractive index decrements as proportional to the ratio of the attenuation coefficient value for the full brain from reference[6] and the density of the grey or white matter values reported in reference [7] (i.e. $\delta_{GM,WM} = \frac{\mu_B}{\rho_{GM,WM}}\delta_B$). In contrast, my second model considered the refractive index decrement as solely proportional to the ratio between the attenuation coefficient value for the full brain and the value corresponding to either the grey or white matter attenuation coefficients (i.e. $\delta_{GM,WM} = \frac{\mu_B}{\mu_{GM,WM}}\delta_B$).

3 Current results

3.1 Simulating a single monomorphic cylinder

I solved the TIE in two-dimensions using the projection approximation to establish my initial conditions. My method applies the fourth order Runge-Kutta evolution algorithm I described earlier to propagate the intensity and phase of the monochromatic scalar electromagnetic wave-field over a total distance of 1 meter. Originally my code discretised a two-dimensional space as an x array with 1024 points and a y array with 512 points. I first attempted to solve the TIE in Fourier space. To calculate the wave-field's derivative terms in equation (1) I use the Fourier derivative theorem to write the derivatives. I also defined functions describing the geometry and optical properties (i.e. refractive index: $\delta(x, y, z)$ and $\mu(x, y, z)$) of the simulated cylinder. Both δ and μ functions use a sigmoid function with adjustable gradient to slightly blur the edge of the cylinder and avoid instability while solving the integrals in equations (2) and (3). My method was slow due to the Fourier derivatives and the output intensity profile after propagation did not appear very stable. I adjusted the ratio of the spacings in my discretised space several times to make sure that the Nyquist mode of the TIE was resolved adequately. Eventually I managed to get a smooth looking intensity profile.
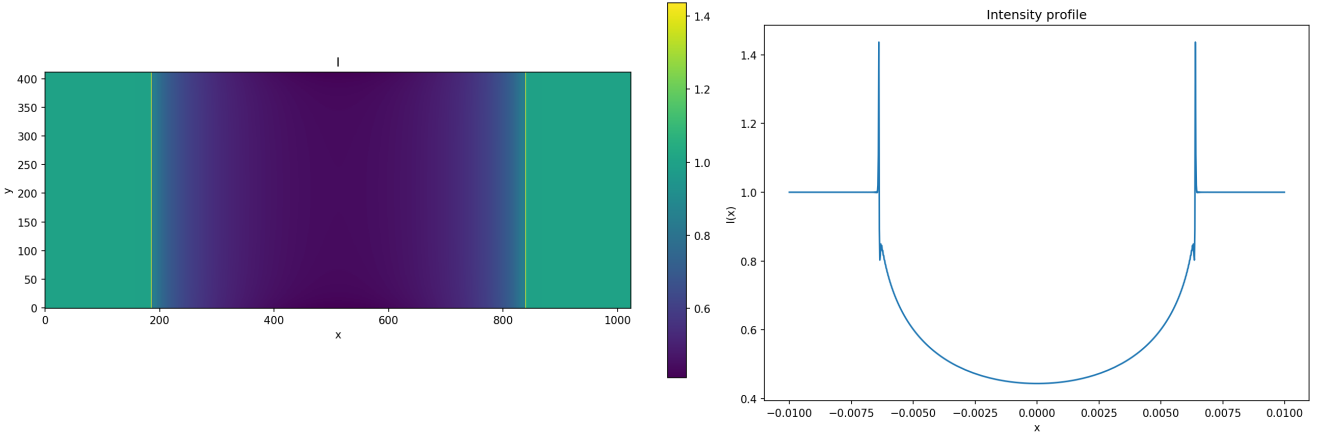
Figure 1: This phase contrast image and phase contrast cross section were the best results I obtained from my Fourier TIE method. Unfortunately my Fourier method was not able to simultaneously match the expected phase contrast peak height given this energy and sample material parameters while at the same time remaining stable. The parameters used to obtain this image were an X-ray energy equal to 22.1629keV (corresponding to a Ag k-alpha 1 source), the cylinder's material was water which has a refractive index decrement $\delta = 468.141$nm while the attenuation coefficient is $\mu = 64.38436$m^{-1}. The cylinder's radius was $R = 6.375$mm. The sigmoid function blurred 0.5 pixels over the edge of the imaged cylinder. The propagation distance used was $z = 1$m.

After obtaining this result I decided partially to change my approach and at the suggestion of my supervisor I solved the TIE in position space with finite differences. I use `numpy.gradient` for the derivative terms and `scipy.ndimage.laplace` for the phase Laplacian term in the TIE. This time my code discretised the two-dimensional space as an x and a y array each with 1024 points. After these changes I was able to understand the probable underlying reason why my Fourier method didn't work even though in theory it should have, given that it is accurate to infinite order[8][9]. The issue was due to an effect known as Gibbs phenomenon, this effect occurs when the nth partial sum of a Fourier series undergoes large oscillations near regions with jump discontinuities[10]. Discovering that higher degree polynomial interpolation does not always improve accuracy was interesting and certainly unexpected.
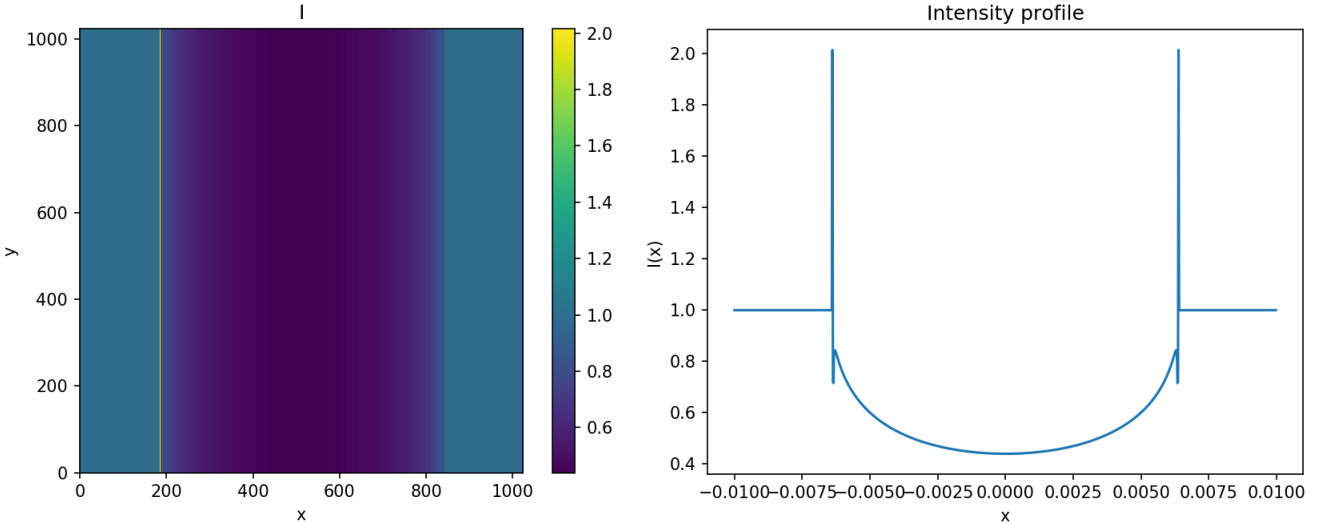

Figure 2: This phase contrast image and phase contrast cross section were obtained using my Finite differences and Runge-Kutta propagation method . As it can be seen here the phase contrast peaks are much higher than the profile found using the Fourier method. The parameters used to obtain this image were an X-ray energy equal to 22.1629keV (corresponding to a Ag k-alpha 1 source), the cylinder's material was water which has a refractive index decrement $\delta = 468.141$nm while the attenuation coefficient is $\mu = 64.38436$m^{-1}. The cylinder's radius was $R = 6.375$mm. The sigmoid function blurred 0.14 pixels over the edge of the imaged cylinder. The propagation distance used was $z = 1$m. The apparent asymmetry of the two-dimensional phase contrast image is due to aliasing.

This result actually presented an apparent improvement in the height of the expected phase contrast fringes. I decided to test my code more thoroughly and made sure that all input parameters were the same as those used in the code my supervisor provided me with to do some output comparisons. According to my supervisor, my contribution to the TIE method propagation using Runge-Kutta is quite significant and he plans to keep using it to improve future simulations of the TIE.

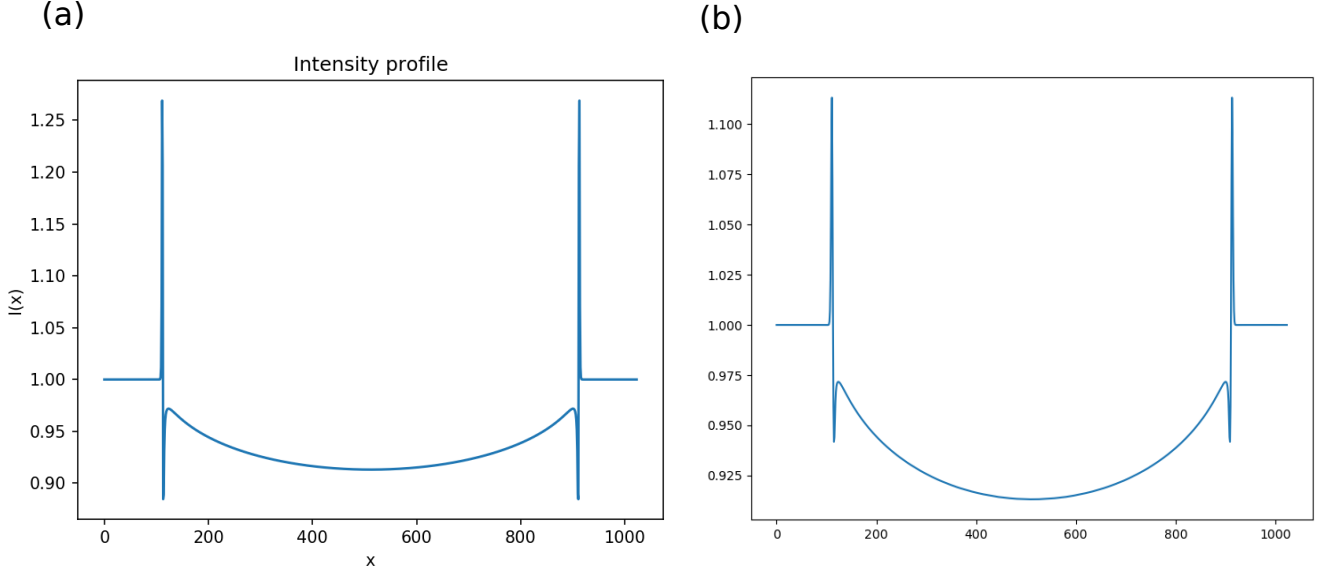## 3.2 Testing if Runge-Kutta propagation increases phase contrast

(a)

(b)

Figure 3: These phase contrast cross sections were obtained by testing: (a) my Finite differences and Runge-Kutta propagation method and (b) the angular spectrum formulation method as the `xri.sim.propAS()` function created by the X-ray imaging group. The input parameters and spatial discretisation codes were identical in both (a) and (b) tests. The parameters were for a single cylinder with a radius of $R = 2$mm. The sample material was water at a density of 1gcm^{-3} and the X-ray energy used was 50keV. I used the "X-ray attenuation calculator" to find the refractive index decrement $\delta = 92.1425$nm and an attenuation coefficient $\mu = 22.69615$m^{-1}. In Figure (a), the sigmoid function blurred 0.14 pixels over the edge of the imaged cylinder. The spatial discretisation arrays used in (a) and (b) were x and y arrays of size 1024 each and of pixel size 5μm. The propagation distance used was $z = 1$m.

3.3 Simulating a couple of concentric monomorphic cylinders

3.3.1 Density difference test: Water and Ice

To test the density dependence of phase contrast I first used a couple embedded concentric sample of two cylinders with the outer most one made of water and the inner most one made of ice.
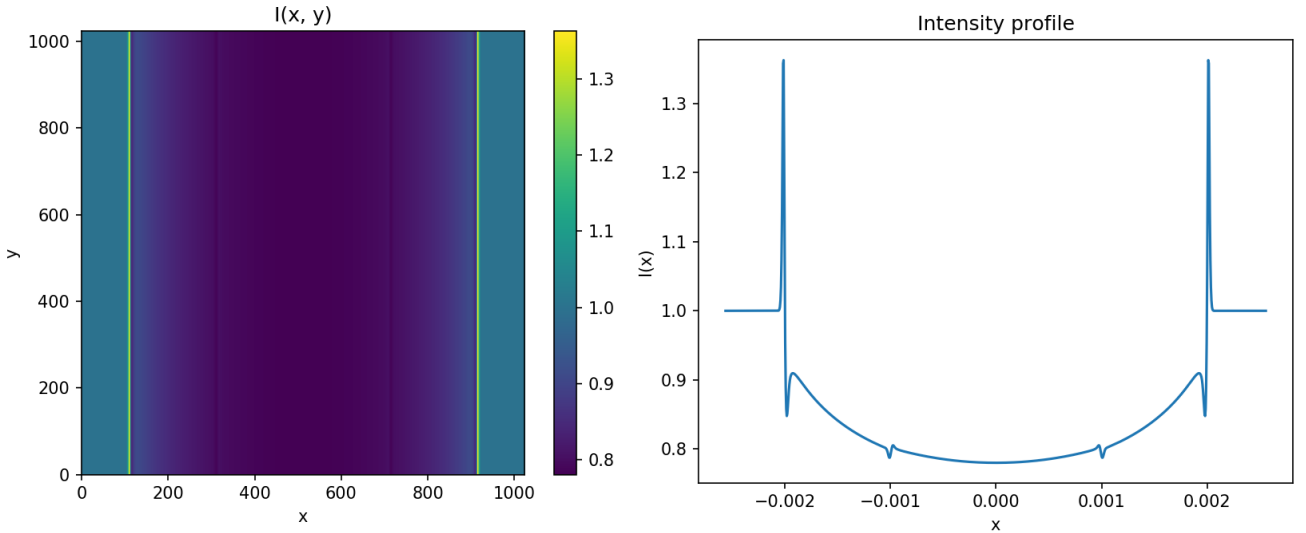

Figure 4: This phase contrast image and phase contrast cross section were obtained with the angular spectrum formulation method as the `xri.sim.propAS()` function created by the X-ray imaging group. The X-ray energy used in this simulation was $E = 22.1629$keV. The water cylinder has a refractive index decrement $\delta_W = 469.337$nm, under this energy the attenuation coefficient of water is $\mu_W = 64.55083$m^{-1}. The ice cylinder has a refractive index decrement $\delta_I = 431.790$nm and attenuation coefficient $\mu_I = 59.38677$m^{-1}. The density difference between these materials is $\Delta\rho = 0.08$gcm^{-3}. The cylinder's radii were $R_W = 2$mm and $R_W = 1$mm. The propagation distance used was $z = 2.5$m.

Another simulation I made for this test takes into account the apparatus parameters and the resolution of the

detector used in my supervisors lab. The plan was to test these results experimentally, but given that the phase contrast fringes observable in the simulations were so small, we decided against testing this in the lab.
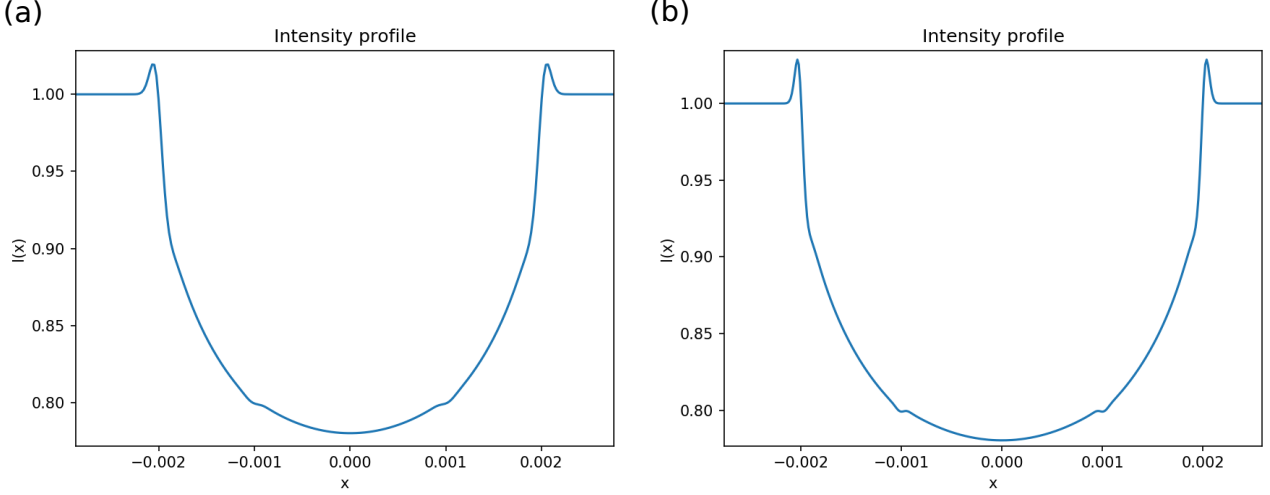
(a)

(b)

Figure 5: This phase contrast cross section was obtained with most parameters being equal to those in the simulation above, except that this time I made some conversions in the spatial discretisation parameters (i.e. x and y arrays), for the conversions I took account the most likely magnification factors we would use for figure 4(a) the magnification factor is 2.5X, for figure 4(b)the magnification factor is 4.0X. I made sure that the dimensions of the spatial arrays and the pixels I used in this simulations matched those of the photon counting detector we will use in the lab. doing this guarantees that the pixels in the object plane are adequately sized given the expected size of the pixels in the detector plane. The effective propagation distance is also inversely scaled by the magnification.

3.3.2 Density difference test: Grey matter and white matter

In this simulation I assume that grey and white matter have the same chemical compositions but distinct densities
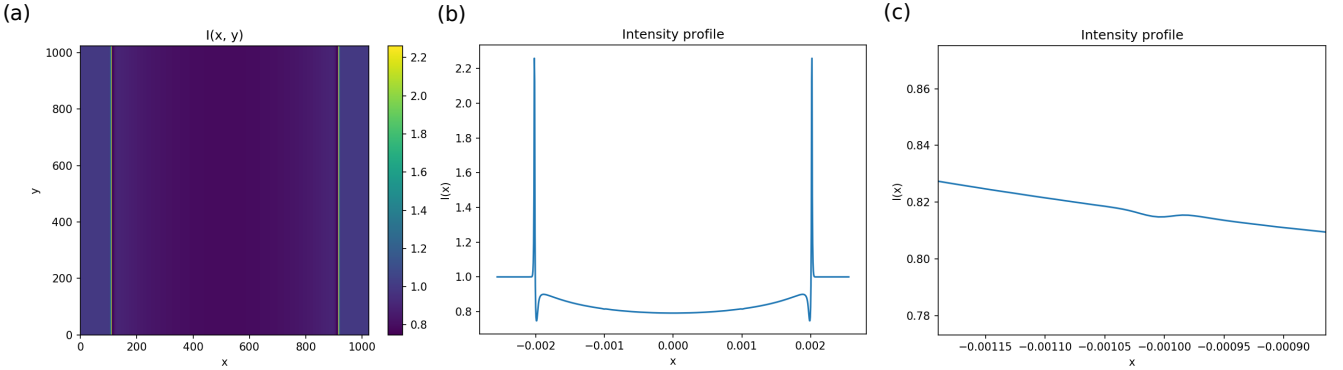
(a)
(b)
(c)

Figure 6: This phase contrast image and phase contrast cross section were obtained with the angular spectrum formulation method as the `xri.sim.propAS()` function created by the X-ray imaging group. The X-ray energy used in this simulation was $E = 24$keV. The water cylinder has a refractive index decrement $\delta_{GM} = 413.45$nm, under this energy the attenuation coefficient of grey matter is $\mu_{GM} = 58.2978$m^{-1}. The white matter cylinder has a refractive index decrement $\delta_{WM} = 411.87$nm and attenuation coefficient $\mu_{GM} = 58.0747$m^{-1}. The density difference between these materials is $\Delta\rho = 0.08$gcm^{-3}. The cylinders' radii were $R_{GM} = 2$mm and $R_{WM} = 1$mm. The propagation distance used was $z = 2.5$m.

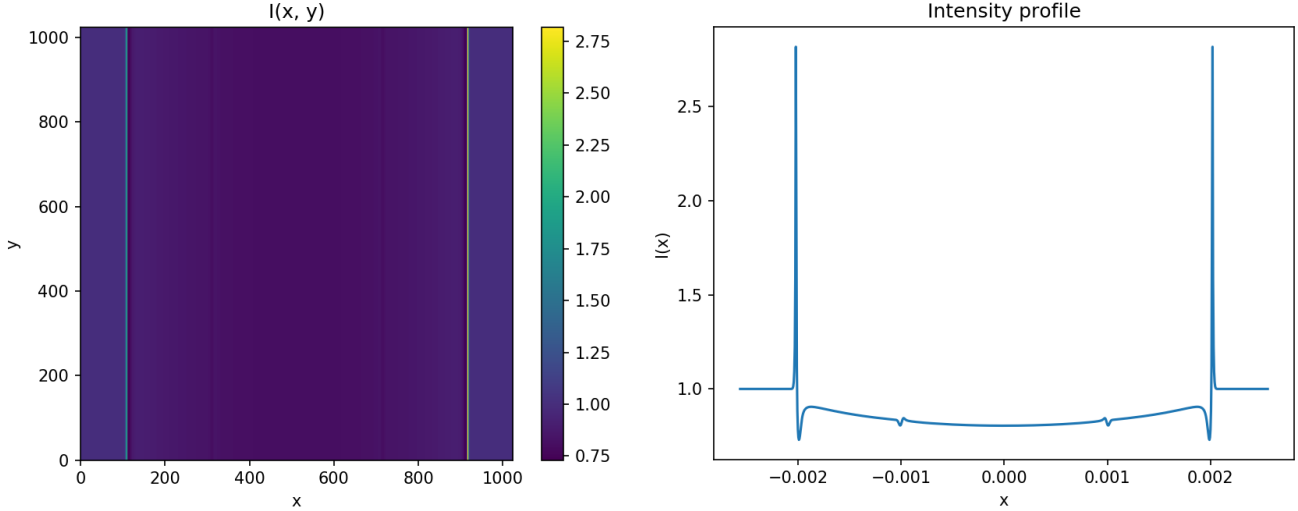### 3.3.3 Chemical difference test: Grey matter and white matter

Figure 7: This phase contrast image (a) and phase contrast cross section (b)(c) were obtained with the angular spectrum formulation method as the `xri.sim.propAS()` function created by the X-ray imaging group. In figure (c) it can be seen that the phase contrast fringes from the inner cylinder are extremely small but can still be observed when the image in (b) is amplified enough. The X-ray energy used in this simulation was $E = 24\text{keV}$. The water cylinder has a refractive index decrement $\delta_{GM} = 459.1\text{nm}$, under this energy the attenuation coefficient of grey matter is $\mu_{GM} = 52\text{m}^{-1}$. The white matter cylinder has a refractive index decrement $\delta_{WM} = 426.31\text{nm}$ and attenuation coefficient $\mu_{GM} = 56\text{m}^{-1}$. The cylinders' radii were $R_{GM} = 2\text{mm}$ and $R_{WM} = 1\text{mm}$. The propagation distance used was $z = 2.5\text{m}$.

To do these two tests I verified that the my calculated theoretical and experimental μ values of grey and white matter do not match. Which lead me to find distinct values of δ for both tests. This mismatch was probably because in the density difference case test the assumption is that there are no chemical differences at all between grey and white matter but this is likely not true. My supervisor and I decided that I should continue using the chemical difference test parameters in future simulations, because this data will help compensate for chemical composition differences. I will have to test the density difference case further with these parameters.

4 Future Plans

I aim to finish my simulations by creating a graphic user interface (GUI) that allows the user to modify interactively the density parameters of the imaged concentric cylinders in the simulation. The goal is to make a easily operated visual representation of the changes in phase and intensity of the X-rays as they interact with the object in-situ.

My supervisor and I are planning to test an X-ray target made of silver which has been newly obtained for the laboratory apparatus. The plan requires that I make some simulations of phase contrast using the characteristic radiation spectrum of silver and see how the phase contrast fringes behave when isolating monochromatic X-ray fringes and comparing them to each other. My aim is to eventually obtain real laboratory data and analyse it to compare efficacy of the new silver target to that of the classic tungsten target currently used in the apparatus.

5 Conclusion

The present aim of my project is to test in a lab some phase contrast simulations I created to investigate how the phase of incident X-rays changes as the density of a couple of distinct sample materials in an arbitrary imaging system changes. The eventual goal of this simulation is to verify if successful phase retrieval can be done of the imaged objects given their variable densities. In this report I present a brief outline of the theoretical perspective of coherent X-ray imaging, a description of my current progress and future aims.

References

[1] Paganin D and Pelliccia D. Tutorials on x-ray phase contrast imaging: Some fundamentals and some conjectures on future developments, 2019. [Online; accessed 25-July-2021].

[2] Press W H et al. *Numerical Recipes 3rd Edition: The Art of Scientific Computing*. Cambridge University Press, 3 edition, 2007.

[3] Goodman J W. *Introduction to Fourier Optics.* JMcGraw-Hill, 2 edition, 1996.

[4] Beltran M A et al. Interface-specific x-ray phase retrieval tomography of complex biological organs. *Physics in Medicine & Biology*, 56(23):7353, 2011.

[5] Croton L C P et al. In situ phase contrast x-ray brain ct. *Scientific Reports*, 8(11412), 2018.

[6] NIST Standard Reference Database 66. X-ray form factor, attenuation, and scattering tables., 2009. [Online; accessed 11-September-2021].

[7] Hasgall P A et al. It'is database for thermal and electromagnetic parameters of biological tissues., 2018. [Online; accessed 14-September-2021].

[8] Billington C J. State-dependent forces in cold quantum gases. 2019.

[9] Fornberg B. The pseudospectral method: Comparisons with finite differences for the elastic wave equation. *GEOPHYSICS*, 52, 1987.

[10] GIBBS J W. Fourier's series. *Nature*, 59, 1898.